

Article

The Influence of the Multiple Scattering on the Optical Properties of Ag-poly(p-xylylene) Composite Coating

Roman Puzko ^{1,2,*}, Vitaliy Tsvirka ³, Alexey Gusev ⁴, Karen Mailyan ⁴, Anton Mikhailitsyn ⁴, Alexey Glushchenkov ⁴, Artem Vdovichenko ^{5,6} , Yuri Trofimov ³, Ilya Ryzhikov ⁴ and Alexander Merzlikin ^{4,*}

¹ Moscow Institute of Physics and Technology (National Research University), Dolgoprudny, 141701 Moscow, Russia

² All-Russia Research Institute of Automatics, 127055 Moscow, Russia

³ Center of LED and Optoelectronic Technologies of National Academy of Sciences of Belarus, 220090 Minsk, Belarus; vitalii.tsvirko@gmail.com (V.T.); trofimov@inel.bas-net.by (Y.T.)

⁴ Institute for Theoretical and Applied Electromagnetics, Russian Academy of Sciences, 125412 Moscow, Russia; 4839356@mail.ru (A.G.); k.mailyan@gmail.com (K.M.); krak1111@gmail.com (A.M.); lex.00.sond@gmail.com (A.G.); nanocom@yandex.ru (I.R.)

⁵ National Research Center “Kurchatov Institute”, 123182 Moscow, Russia; vdartem@ya.ru

⁶ N.S. Enikolopov Institute of Synthetic Polymeric Materials, Russian Academy of Sciences, 117393 Moscow, Russia

* Correspondence: roman998@mail.ru (R.P.); merzlikin_a@mail.ru (A.M.)

Received: 11 September 2020; Accepted: 6 October 2020; Published: 14 October 2020



Abstract: The creation of composite coatings with assigned optical properties is an important problem of modern science and technology. We have considered the metal-polymer nanocomposites based on poly(p-xylylene), with various concentrations of plasmon components—silver nanoparticles. We have carried out the optical measurements of the reflection, transmission, scattering and absorption coefficients for the manufactured films. We have retrieved the effective optical parameters of the composite coatings. The theoretical estimations based on the scattering and absorption data show that the scattering effectively occurs on the clusters of metal nanoparticles. This significantly influences the optical properties of the composite coating.

Keywords: nanocomposite; light scattering; plasmonic nanoparticles

1. Introduction

The design and manufacturing of composite materials with unique physical and chemical properties are of great interest to the scientific community [1,2]. The microstructure of composite materials provides them with properties (thermal conductivity, electrical conductivity, dielectrical permittivity and/or magnetic permeability, elasticity, etc.) that are qualitatively different from those of natural materials.

The metal-polymer composites are the prospective composite materials. Their microstructure is a dielectric matrix with metal inclusions. The metal-polymer composites show a number of unusual physical properties [3–7]. The nanocomposite properties significantly depend on the concentration, size and shape of metal inclusions. Moreover, the positions and shapes of boundaries between the structural components noticeably influence the material properties. The choice of metal component allows the additional tuning of composite properties. The metal-polymer composites with the immersed plasmonic nanoparticles have great potential for the applications: plasmonic metals are widely used for various purposes, such as on-chip optical devices [8], sensors with high sensitivity [9,10] and surface plasmon-polaritons lasers [11].

Poly(p-xylylene) (PPX) is the appropriate material as the material of a polymer matrix. The manufacturing of PPX coatings is based on the cryochemical synthesis of a polymer material from p-xylylene monomer [12]. The synthesis of the polymer material occurs as a result of the polymerization of the monomer molecules condensed on the substrate. The metal-polymer composite based on the PPX is produced by deposition of the sublimated metal on the substrate, together with the p-xylylene monomer. Notably, the coatings formation occurs in the process of self-assembly, without involving additional techniques.

The specific parameters of the manufacturing process influence the microstructure of metal-polymer composites. The remarkable feature of the metal-polymer coating manufacturing is the interaction between the polymerizing monomer and the metal particles, i.e., the processes of monomer polymerization and metal crystallization affect each other [13,14]. In particular, the presence of the polymer component prevents the aggregation of metal particles. At the same time, the process of the polymer matrix formation occurs under the influence of the metal inclusions. The resulting microstructure of the composite material is the result of two simultaneous processes: the polymerization of dielectric matrix and the aggregation of the sublimated metal particles. The spatial distribution of metal nanoparticles inside the coating can be significantly nonuniform, which is manifested in the value of the percolation threshold [15].

The scattering properties of metal-polymer coatings microstructure is of particular interest due to the complex morphology. Namely, the PPX coating is formed by the polymer material globules with the size ~ 100 nm, which are separated by the spacings with metal nanoparticles. The light propagation through the coatings is accompanied by both the absorption and scattering processes.

It should be noted that two types of scattering problems can be distinguished: scattering by the roughness of half-space/layered structure [16–19] and scattering by the volumetric inclusions of the medium [20–22].

As a rule, the authors consider scattering in the approximation of small-sized (in comparison to the wavelength) inhomogeneities/roughness. The small size of fluctuations allows one to construct a perturbation theory [18] or an equivalent method of the stochastic functionals [19]. The scattering theory can be constructed, which is based on the multipole expansion of the inclusions electromagnetic responses [22]. Generally, the scattering theories are limited to the single and the double scattering processes, which allow one to describe the distinguishing features of the scattered radiation (the Yoneda peaks [23], the resonant scattering in systems with modes [22,24], etc.). At the same time, the multiple scattering in the percolation films is of considerable interest [25]. The anomalous scattering of light on the surface of metal-dielectric films was investigated earlier in the presence of collective plasmon resonance [26,27]: the field localization occurs at some points on the percolation film.

This work is devoted to the metal-polymer coatings based on the poly(p-xylylene) matrix with the immersed nanoparticles of silver (PPX+Ag composites). The previously developed method [12] of the PPX coatings production is based on the use of polymerization of p-xylylene from the gas phase. The manufacturing of the PPX+Ag composite is a developed technology that opens up the opportunity to produce the metal-polymer coatings [4,28–30]. The method of cryochemical synthesis of PPX with simultaneous sublimated silver deposition makes it possible to produce metal-polymer coatings with different silver volume concentrations [28–30].

The structure of the considered composite is a polymer matrix (PPX) with the immersed plasmonic silver particles, which tend to form agglomerates in the manufacturing process. The particles agglomerates are able to act as the centers of collective light scattering, which is an important feature observed in the percolation films. In contrast to the films considered in [26,27], the light scattering occurs inside of the composite sample. Being the object of higher dimension, the PPX+Ag composite coating contains the scattering centers similar to those of percolation films. The field localization can occur inside the particles clusters. In this connection, the nature of light scattering in such a system is an intriguing research question.

This work is devoted to the development of the manufacturing methods of the metal-polymer coatings based on PPX, as well as to the characterization of the coatings morphology and their optical

properties. In particular, the scattering features of PPX coatings with different volume concentrations of silver (from 3.5 to 10% of the volume) are studied. The question is of particular interest as soon as the increase of plasmon particles concentration leads to the multiple light scattering and violations of the effective medium approximations.

2. Materials and Methods

2.1. The Manufacturing of the PPX+Ag Coatings

The manufacturing process of a PPX composite coating with immersed silver particles is the cryochemical polymerization of PPX in vacuum with the simultaneous deposition of silver particles (see Figure 1). The materials deposition takes place inside a vapor deposition polymerization chamber at the pressures below 10^{-5} Torr. The initial stage of the process is the sublimation of the cyclic dimer of p-xylylene (CDPX). During the pyrolysis of sublimated dimer at ~ 670 °C, the p-xylylene monomer is obtained [12]. The monomer is cooled and condensed onto a prepared glass substrate. The substrate is cooled to -196 °C by liquid nitrogen. The monomer is metastable at this temperature [31,32]. The simultaneous deposition of the silver particles on the substrate is performed. The silver particles are produced by thermal evaporation of silver powder by the Knudsen effusion cell. Then, the co-condensate is slowly heated. During the heating process, the monomers of p-xylylene polymerize into PPX, and aggregates of silver nanoparticles are formed from clustered and atomic silver.

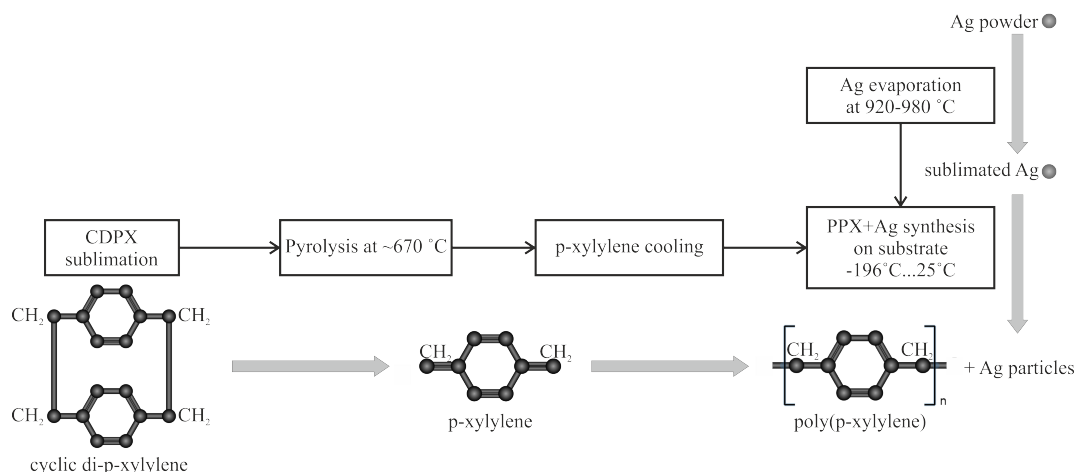


Figure 1. The scheme of poly(p-xylylene) (PPX)+Ag coating manufacturing.

The series of nanocomposite coatings with a silver volume concentration from 2 to 50% was produced. The coatings with the concentrations above 12–14% are cracked. This is explained by the fact that polymerization occurs at sufficiently low temperatures (-110 °C ... -70 °C) and composites with higher filling factor have insufficient mechanical strengths to withstand the stresses which appear at low-temperature synthesis.

2.2. The Molecular Weight Fraction and the Samples Morphology

The produced samples were studied by IR spectroscopy and thermogravimetric analysis (TGA). In order to test the capability of the coatings reproduction in the manufacturing process, several samples with the same silver concentration were synthesized. The TGA measurements made for pairs of samples with the same silver concentration show almost the identical processes of thermal degradation of the samples (see the Supplementary Materials). In situ measurements of resistance dependences during the synthesis were performed, as well as the measurements of UV spectra of the obtained coatings. The results turned out to be identical, which indicates that the technology allows perfect control of the

synthesis conditions and the production of samples with assigned parameters. The morphology of PPX coatings with different volume concentrations of silver were studied with a SEM microscope.

2.3. The Investigation of the Samples Optical Properties

The optical properties of PPX+Ag nanocomposites deposited on glass were measured in transmission and reflection geometries by means of integral method (using an integrating sphere). A 70 W halogen lamp with an operating current of about 7 A was used as a radiation source. The lamp supply current was maintained with an accuracy of $\pm 1\text{ mA}$. The measurements were performed using a CAS 140CT CCD spectroradiometer (Instrument Systems GmbH) with the integrating sphere ISP80 as the optical probe. The measurements were performed in the spectral range 380–1000 nm for the normal light incidence.

The sample was placed at the entrance port of the integrating sphere in the transmission geometry. The diameter of the entrance port is 15 mm; the diameter of the sphere is 80 mm. An exit port with diameter 6.6 mm was located coaxially with the entrance port on the opposite side of the sphere. Thus, the source radiation concentrated in a solid angle corresponding to a linear angle less than 4.7° passed freely through the sphere. The rest of the radiation was recorded by a photodetector as scattered radiation. A collimator was used to form a narrow light beam, the spot diameter was about 4 mm at the exit from sphere. The part of the lamp radiation, concentrated in an angle of more than 4.7° , was taken into account by subtracting it from the measurement result. The values of the total transmittance of the samples with a closed exit port of the sphere were also obtained.

The integrating sphere and the sample were rotated by 180° in the reflection geometry, i.e., the light entered the sphere through a port with the diameter 6.6 mm. Thus, the diffuse reflection was measured at normal incidence of light on the sample, since the specularly reflected radiation exited through the 6.6 mm port. The total reflection was measured in the configuration with the sample rotated by 8° . The sample was rotated by the replacing of the flat flange of the integrating sphere 15 mm port with the wedge-shaped one.

The absorption coefficient of the sample was calculated by using the spectral dependences of total transmission and total reflection coefficients.

2.4. The Retrieval of the Samples Effective Optical Parameters

The effective refractive index was retrieved by the numerical analysis of the reflection and transmission coefficients for the coatings with different volume concentrations of silver. The parameters were obtained by minimization of the discrepancy between the experimental reflection and transmission coefficients and the theoretical ones. The specular reflection coefficient was calculated as the difference between the total reflection coefficient and the diffuse reflection coefficient measured in the experiment. The theoretical model of the system was used for calculations of the theoretical reflection and transmission coefficients. The model was composed of composite material layer placed on the glass substrate. The reflection and transmission coefficients were calculated by means of the transfer matrix approach [33]. Thus, two input parameters were used to find the parameters of the material for each wavelength. The residual S , which was used as the discrepancy measure, was defined for a single wavelength, as follows

$$S(n_1, n_2) = |R_{exp} - R_{th}(n_1, n_2)| + |T_{exp} - T_{th}(n_1, n_2)|, \quad (1)$$

where R_{exp} (T_{exp}) and R_{th} (T_{th}) are the experimental and theoretical dependences of the reflection (transmission) coefficients. The fitting parameters of the numerical procedure were the real (n_1) and imaginary (n_2) parts of the effective refractive index of the coating. The Nelder–Mead method was used to minimize the residual given by Equation (1). That is, the inverse problem was solved in order to retrieve the parameters of the composite coatings. As a result, the dispersion curves were obtained for PPX+Ag coatings with different silver concentrations.

The SEM data on the coatings thickness were used for the parameters retrieval. The thickness of the coatings with the different silver concentrations varied in the range from 300 to 800 nm. Thus, the SEM measurements allow one to reduce the number of adjustable parameters. The knowledge of the coatings thicknesses significantly increased the reliability of the parameters retrieval procedure.

The solution to the inverse problem of parameters retrieval is influenced by the variations of the thickness. The reflection R and transmission T coefficients depend on the thickness of the composite film. As a result, the retrieved parameters depend on the film thickness used in the model, i.e., the accuracy of the defined parameters depends on the derivatives dR/dh and dT/dh and the variation of thickness h . The variation of the thickness defined in the measurements was approximately $\pm 10 - 25$ nm for different samples. That uncertainty results in the variations of the order $\pm 0.015 - 0.038$ for the real part and $\pm 0.008 - 0.020$ for the imaginary part of the retrieved refractive index.

The optical measurements were performed for the pairs of the samples with the same silver concentrations. However, the measured spectra and the retrieved effective parameters are in close agreement with each other, i.e., the difference between the retrieved parameters is close to the uncertainty due to the variations of samples thicknesses.

3. Results and Discussion

3.1. Molecular Weight Fraction and the Infrared Spectra

According to the TGA data for samples in air flow (see Figure 2), the pure PPX coatings remain stable up to 220 °C, while the nanocomposites remain stable only up to 100 °C. The composites lose up to 15% of their mass at the temperature 220 °C. This indicates, firstly, an increase in the low molecular weight fraction, and secondly, the negative effect of silver on the oxidative stability of the composite samples in comparison to the pure polymer material. The concentration of the low molecular weight fraction, which increases with the silver concentration, leads to the deteriorating mechanical properties. That leads, consequently, to the cracking of the samples with the high filling factor. The obtained TGA data are helpful for developing of conditions for post-processing of nanocomposite coatings by means of the annealing.

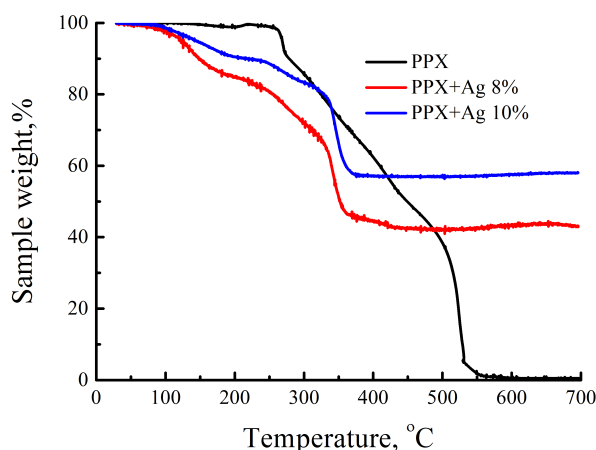


Figure 2. The thermogravimetric measurements of PPX+Ag coatings with different concentrations of silver in air flow.

The IR spectra of the nanocomposite samples are similar to those of the pure PPX polymer (see Figure 3). The new bands appear in the spectra of PPX+Ag composites in comparison with the spectra of polymer matrix. In particular, the intense band appears in the range 1378–1390 cm^{-1} , which indicates the symmetric stretching vibrations of the carboxylate group (COO^-) adsorbed on the surface of silver nanoparticles [34]. New bands with maxima at 1260, 1380 and 1700 cm^{-1} in the spectra of nanocomposites can be attributed to various oxygen-containing groups.

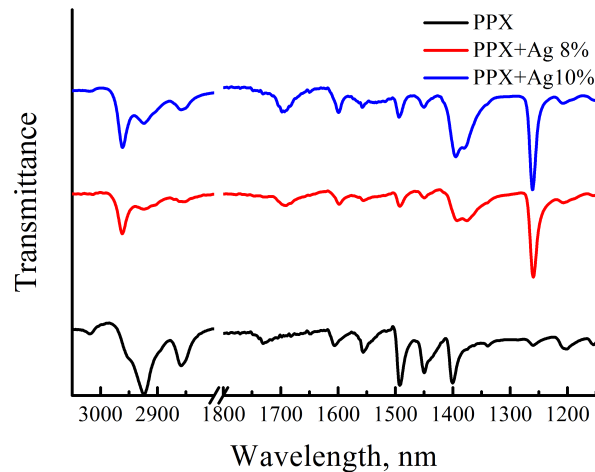


Figure 3. The infrared spectra of PPX+Ag coatings with different concentrations of silver.

3.2. Morphology of the Samples

The morphology of PPX coatings with different volume concentrations of silver were studied with a SEM microscope (see Figure 4). The surface of the coating acquires a strongly inhomogeneous structure when the silver particles concentration increases. The structural defects of the coatings indicate the presence of PPX globules about 100 nm in size. The SEM image of coating with 8% silver concentration shows the presence of large particle aggregates on the surface. The coatings with higher silver concentration acquire large defects—the cracks with a characteristic size exceeding the size of the polymer globules.

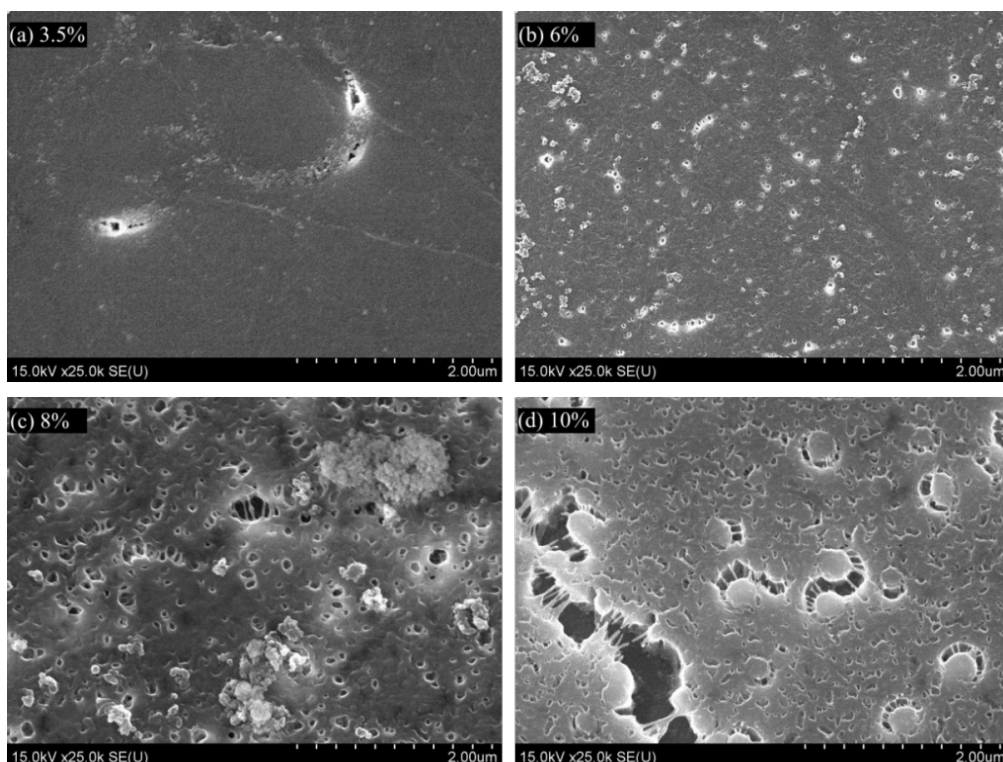


Figure 4. SEM images of PPX+Ag composite coating with (a) 3.5%, (b) 6%, (c) 8%, (d) 10% volume concentration of silver.

3.3. Optical Measurements

The optical measurements were carried out for the samples with different silver concentrations: 3.5%, 6%, 8% and 10% (see Figure 5). A significant part of radiation in the wavelength range of 400–700 nm is absorbed inside the films. At the same time, most of the radiation transmitted through the coatings is the scattered light (see Figure 6). Therefore, a dip in the value of the transmission coefficient is observed in this wavelength range. However, the absorption coefficient decreases with the increase of wavelength. The scattering coefficient increases for the samples with a silver concentration 6%, 8%, and 10%. The optical measurements show that the largest scattering is observed for sample with 8% of silver. The scattering coefficient is lower for the sample with 10% silver concentration, however, the absorption coefficient is higher. The light extinction due to the absorption and the scattering in the sample with 10% of silver leads to almost zero specular transmission in the wavelength range of 400–700 nm.

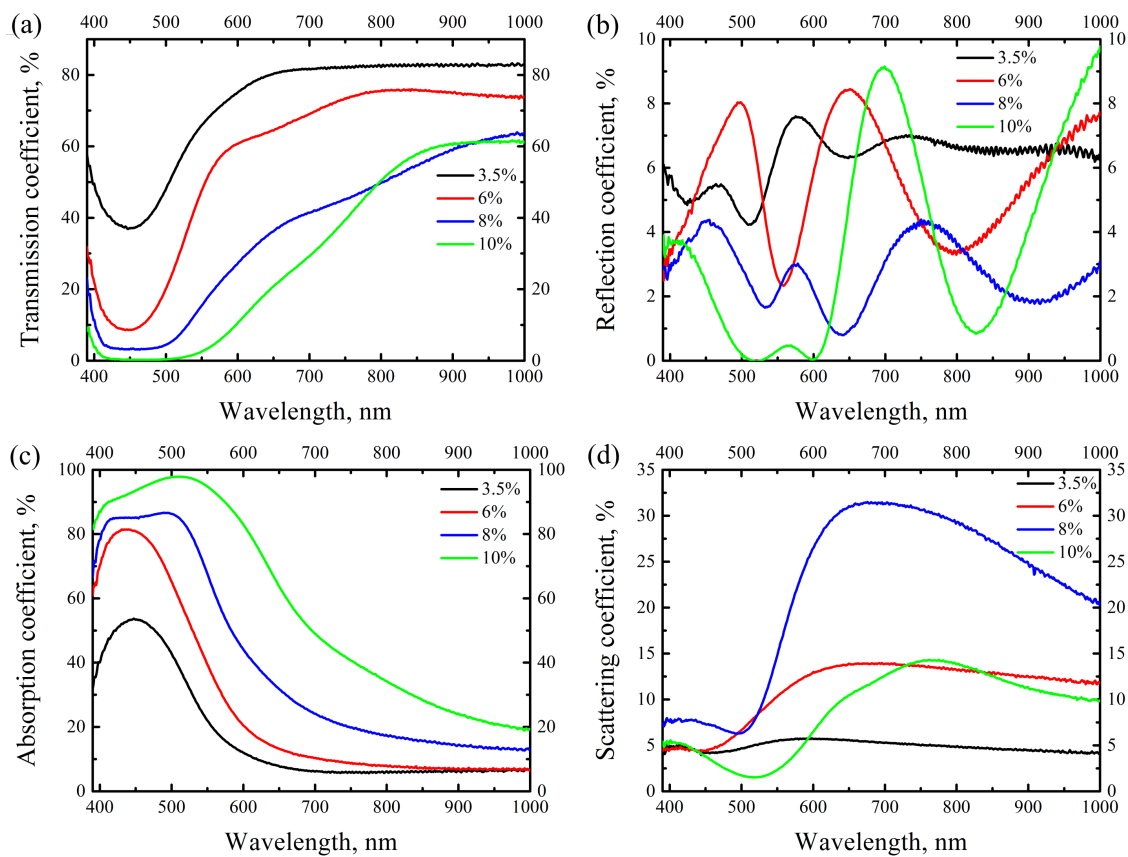


Figure 5. The dependences of the coefficients of (a) transmission, (b) reflection, (c) absorption, and (d) scattering for the PPX+Ag coatings with the different volume concentrations of silver (3.5%, 6%, 8%, 10%) at normal incidence.

According to studies carried out in [22], the scattering coefficient increases due to an increase in the field inside the scattering coating in the case of single scattering by small inhomogeneities. However, the field increase in this case should lead to the increase in the absorption coefficient in the film. Thus, the measured dependences of the scattering and absorption coefficients (see Figure 5c,d) indicate the collective nature of scattering or/and the significant change in the scattering and absorption cross sections of silver particles.

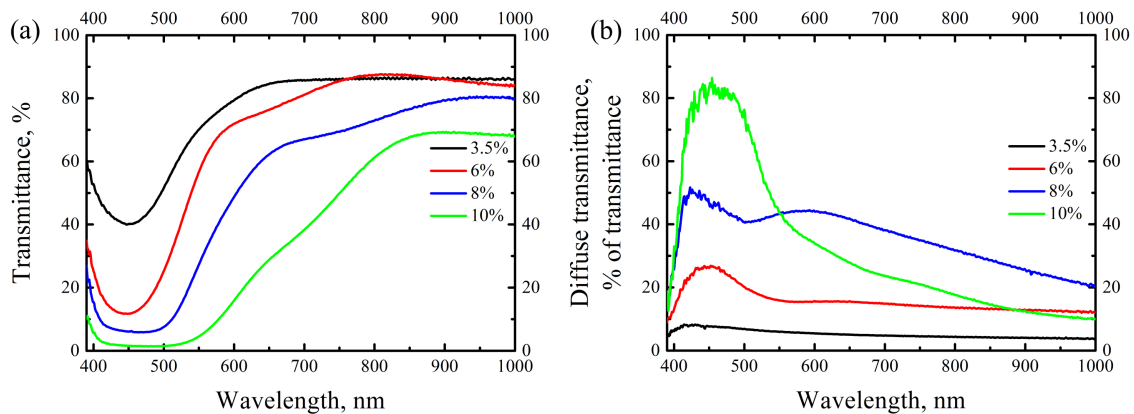


Figure 6. The dependences of (a) the total transmittance, (b) the diffuse transmittance (in % of total transmittance) on the wavelength for the PPX+Ag coatings with the different volume concentrations of silver (3.5%, 6%, 8%, 10%) at normal incidence.

3.4. The effective Parameters of the Composite Coatings

The Figure 7 shows the dispersion dependences of the imaginary part of the effective refractive index for PPX+Ag coatings with different silver concentrations. The calculations show that the n_2 coefficients of the composite coatings with silver concentrations of 6%, 8%, and 10% are significantly higher than the values for coating with 3.5% silver. The imaginary part of the effective refractive index has a maximum in the wavelength range from 450 nm to 550 nm for all of the coatings. The position of the maximum shifts to longer wavelengths with the increase of the silver concentration.

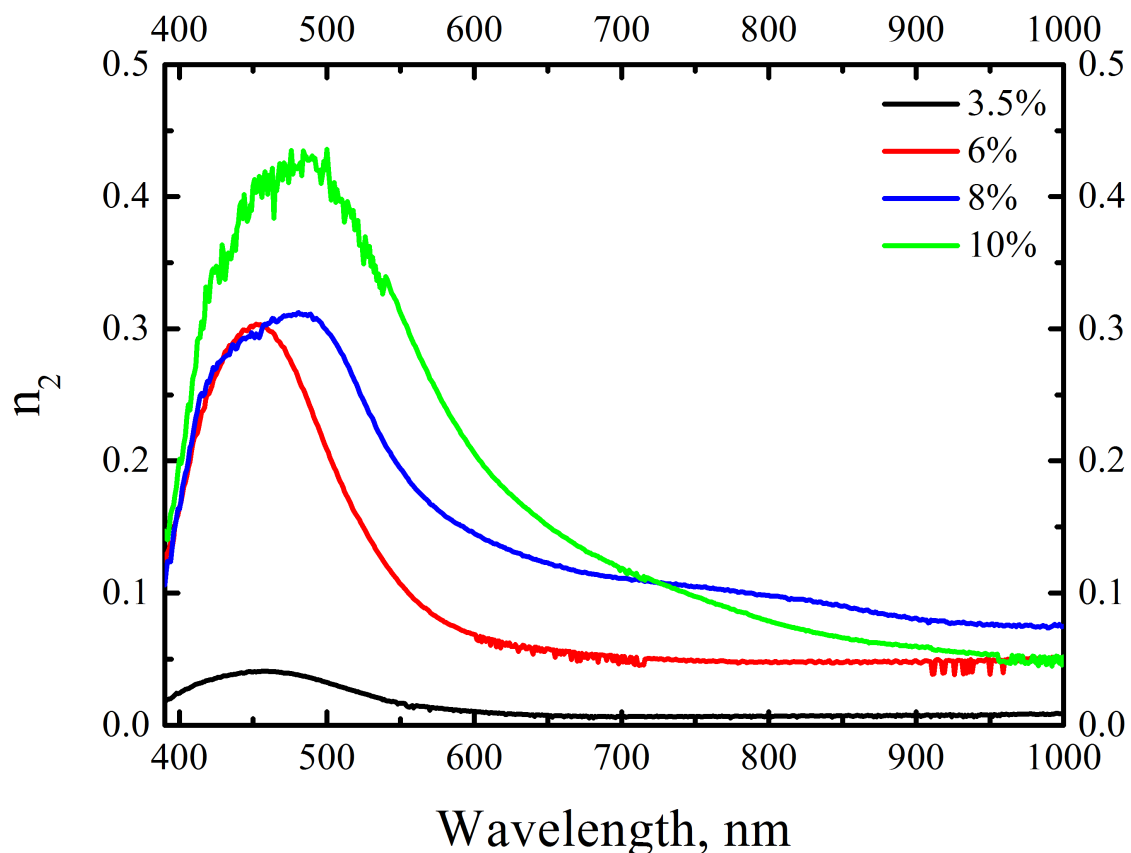


Figure 7. The imaginary part of the effective refractive index of PPX+Ag composite with different volume concentrations of silver: 3.5% (black), 6% (red), 8% (blue), 10% (green).

The physical meaning of the imaginary part of the effective refractive index should be noted. As the coherent light beam propagates through the PPX+Ag composite, some part of the coherent light energy is scattered and some part is absorbed by metal nanoparticles. As a result of these processes, the incident radiation is partly scattered and partly absorbed. The imaginary part of the effective refractive index describes the decay of the coherent wave inside the coating, i.e., it describes the processes of absorption and scattering in the case of the PPX+Ag composite.

The increase of the volume concentration of silver is accompanied by the increase of the concentration of scattering and absorbing centers. As a result, the imaginary part of the effective refractive index should increase. The coherent radiation intensity I decays with the length of the propagation. Within the first approximation of the transport equation, when the single scattering is considered only, the change of the intensity dI after the propagation through the path dz is as follows

$$dI = -IN\sigma_{ext}dz = -IN(\sigma_{sc} + \sigma_{abs})dz, \quad (2)$$

where N is the concentration of inclusions, and σ_{ext} , σ_{sc} , σ_{abs} are the extinction, scattering and absorption cross sections, respectively. Hence, the imaginary part of the effective refractive index can be estimated as follows

$$n_2 = \frac{1}{2k_0}N(\sigma_{sc} + \sigma_{abs}), \quad (3)$$

where k_0 is the wave number. According to Equation (3) $n_2 \sim N$, i.e., the imaginary part of the effective refractive index, increases with the increase of the silver particles concentration. However, according to the parameters retrieved from the experiment, the value of n_2 shows significantly different behavior for the coatings (see Figure 7). Thus, either the scattering and absorption cross sections of the nanoparticles (and their scattering and absorption cross sections) differ for different silver concentrations, or the single scattering model is not applicable for the description of light scattering in the PPX+Ag coatings. In the latter case, it is necessary to take into account that scattering occurs on the clusters of plasmon particles. The field inside such clusters fluctuates, having maxima in the regions of field localization, which was previously studied for the percolation films [35].

The shape of the dispersion curves on Figure 7 indicates clearly the change in the plasmon resonances occurred in the metal fraction. The dispersion curves for the composited with low silver concentrations (3.5% and 6%) have only one smooth peak. This corresponds to the case of scattering by the distant nanoparticles with approximately the same sizes. On the contrary, there are groups of close resonances in the samples with higher silver concentration, which could be explained by the presence of scattering centers with varying sizes. That is, the nanoparticles with different sizes are present in the coating or the light is scattered by the nanoparticles clusters.

3.5. The Scattering Centers of the PPX+Ag Composites

The transmission, reflection, scattering and absorption data can be used for the estimation of the scattering and absorption cross section of the silver particles in the PPX coating. In particular, the experimental data are used to evaluate the scattering nature, i.e., to find out if the light is scattered by the groups of closely placed particles or by the single particles. The important difference between the two regimes is the field distribution in the vicinity of the scattering centers: the near field of plasmonic particles may lead to the field localization in the clusters. The analysis of silver particle field shows that the near field interaction between the particles lead to the plasmonic transport.

Two estimations of the silver inclusions sizes were carried out in order to determine the nature of the scattering process. The following estimations are made in the assumption of the single scattering processes on the distant scattering centers.

The first estimation of the characteristic size of the silver inclusions is based on the study of the scattering and absorption coefficients. The silver nanoparticles inside the PPX coating act both as the scattering and absorbing particles. The scattering/absorption coefficients in films are determined by the magnitude of the electric field in the coating, the concentration of the silver particles, and their

scattering/absorption cross sections. Since the scattering and absorption coefficients depend on the electric field in the system and the concentration of particles in the same way, it is possible to determine the relationship between the scattering cross section and the absorption cross section of the silver particles. The ratio leads straightforwardly to the estimation of the nanoparticles size.

The scattering and the absorption in the material are proportional to the values of $\sigma_{sc}N$ and $\sigma_{abs}N$, respectively, within the first order approximation by particle size. The scattering cross section of a small metallic sphere in the dipole approximation [36] is as follows

$$\sigma_{sc} = \frac{8\pi}{3}k^4|\alpha|^2, \quad (4)$$

where $\alpha = R^3(\epsilon_{Ag} - \epsilon_{PPX})/(\epsilon_{Ag} + 2\epsilon_{PPX})$ is the polarizability of the particle and k is the wave number in the surrounding medium. The absorption cross section of the particle is

$$\sigma_{abs} = 4\pi k \text{Im}(\alpha). \quad (5)$$

The Equations (4) and (5) provide the following relation between the absorption coefficient A and the scattering coefficient S

$$\frac{A}{S} = \frac{\sigma_{abs}}{\sigma_{sc}} = -\frac{3}{2k^3} \text{Im}\left(\frac{1}{\alpha}\right) = -\frac{3}{2k^3 R^3} \text{Im}\left(\frac{\epsilon_{Ag} + 2\epsilon_{PPX}}{\epsilon_{Ag} - \epsilon_{PPX}}\right), \quad (6)$$

which leads to the particle radius estimation from the scattering and absorption coefficients.

From the other side, the characteristic sizes of silver particles can be estimated from the previously retrieved effective parameters of the coatings. The extinction cross section of the particles can be evaluated by considering the attenuation of coherent radiation in the material in the weak scattering approximation. The extinction coefficient was estimated from the imaginary and real parts of the retrieved refractive index in accordance with Equation (3). The equation

$$\sigma_{ext} = \sigma_{abs} + \sigma_{sc} \quad (7)$$

and Equations (4) and (5) led to the particles size estimation.

The particles' characteristic sizes estimated by different methods significantly differ and vary with the wavelengths. That shows that the weak scattering model is incompatible with the experimental data. Thus, the estimates of the particles' sizes indicate the collective nature of scattering in the PPX+Ag films. The significant amount of radiation is either scattered or absorbed in the coating. The observed scattering differs from the scattering by distant nanoparticles. As a result, the effective medium theory is inapplicable for the description of the coatings with high silver concentration.

4. Conclusions

The metal-polymer composites are of great interest as the optical media with assigned parameters (the refractive index, the absorption coefficient, the magnetic properties, etc.) in a wide spectral range. These materials can be used as organic optical elements, waveguides, interference filters, and photonic crystals [28]. Poly(p-xylylene) is a prospective material as the dielectric matrix of metal-polymer composites. Within the framework of this work, a technology for the manufacture of metal-polymer nanocomposites based on a poly(p-xylylene) matrix with various concentrations of plasmon components (silver nanoparticles) was developed. The manufacturing technology is based on cryochemical synthesis and makes it possible to obtain composites with various properties.

The measurements, the transmission, reflection, absorption and scattering coefficients were performed in order to study the optical properties of the coatings in the spectral range 390–1000 nm. The effective parameters of the composite films PPX+Ag were retrieved from the experimental data. The obtained parameters show the significant response of the plasmonic nanocomposite in the wavelength

range of 400–700 nm. The spectral position of the maximum response varies for films with the different concentrations of silver nanoparticles, which provides the opportunity of tuning the coating properties.

The estimates of the characteristic size of silver particles based on scattering and absorption data show that scattering effectively occurs on the groups of closely placed particles, rather than on individual distant particles. Thus, localization of the field may take place in the random clusters of silver particles due to near-field effects. The similar features were previously studied for percolation films [25–27]. The electric field can be significantly inhomogeneous and have a number of local maxima inside the clusters of silver nanoparticles [35]. This issue is of great interest for further research.

Supplementary Materials: The following are available at <http://www.mdpi.com/2079-6412/10/10/976/s1>, Figure S1: The thermogravimetric measurements of PPX+Ag coatings with different concentrations of silver in nitrogen atmosphere.

Author Contributions: Conceptualization, I.R., A.G. (Alexey Gusev), V.T. and A.M. (Alexander Merzlikin); methodology, A.V. and R.P.; software, A.G. (Alexey Gusev) and R.P.; validation, V.T. and A.M. (Alexander Merzlikin); formal analysis, R.P. and A.M. (Alexander Merzlikin); investigation, Y.T., A.M. (Anton Mikhailitsyn), A.G. (Alexey Gusev) and R.P.; resources, K.M., Y.T. and V.T.; data curation, Y.T., A.V. and I.R.; writing—original draft preparation, A.G. (Alexey Gusev), V.T. and R.P.; writing—review and editing, R.P., V.T., A.G. (Alexey Gusev), A.G. (Alexey Glushchenkov), A.V., I.R. and A.M. (Alexander Merzlikin); visualization, R.P.; supervision, A.M. (Alexander Merzlikin); project administration, I.R. and A.M. (Alexander Merzlikin). All authors have read and agreed to the published version of the manuscript.

Funding: This research was funded by the joint grant of Belarusian Republican Foundation for Fundamental Research (no. F18R-248) and Russian Foundation for Basic Research (no. 18-52-00044). R. Puzko and A. Merzlikin acknowledge financial support by the Foundation for the Advancement of Theoretical Physics and Mathematics “BASIS”.

Acknowledgments: Samples were made with ITAE RAS laboratory equipment.

Conflicts of Interest: The authors declare no conflict of interest.

References

1. Cai, W.; Shalae, V.M. *Optical Metamaterials*; Springer: New York, NY, USA 2010; Volume 10.
2. Clyne, T.; Hull, D. *An Introduction to Composite Materials*; Cambridge University Press: Cambridge, UK, 1996.
3. Gusev, A.; Mailyan, K.; Pebalk, A.; Ryzhikov, I.; Chvalun, S. Prospects for the application of nanostructured polymer and nanocomposite films based on poly-p-xylylene for micro-, opto-, and nanoelectronics. *J. Commun. Technol. Electron.* **2009**, *54*, 833–843. [[CrossRef](#)]
4. Boginskaya, I.; Gusev, A.; Mailyan, K.; Ozerin, S.; Pebalk, A.; Ryzhikov, I.; Sedova, M.; Chvalun, S. Structure of and electric conduction in metal–polymer poly-para-xylylene–Ag nanocomposite films. *J. Commun. Technol. Electron.* **2011**, *56*, 66–72. [[CrossRef](#)]
5. Aleksandrova, G.; Prozorova, G.; Klimenkov, I.; Sukhov, B.; Trofimov, B. Effect of metal nanoparticles on the thermal stability and conductivity of nanocomposites. *Bull. Russ. Acad. Sci. Phys.* **2016**, *80*, 49–54. [[CrossRef](#)]
6. Ozerin, S.A.; Vdovichenko, A.Y.; Streltsov, D.R.; Davydov, A.B.; Orekhov, A.S.; Vasiliev, A.L.; Zubavichus, Y.V.; Grigoriev, E.I.; Zavyalov, S.A.; Oveshnikov, L.N.; et al. Structure and magnetic properties of Ni-poly (p-xylylene) nanocomposites synthesized by vapor deposition polymerization. *J. Phys. Chem. Solids* **2017**, *111*, 245–253. [[CrossRef](#)]
7. Khnykov, A.Y.; Vdovichenko, A.Y.; Morozov, P.V.; Zavyalov, S.A.; Shevchenko, V.G.; Chvalun, S.N. Gas-sensing properties of poly (p-xylylene)-Titanium thin film nanocomposite, prepared by vapor deposition polymerization. *Sens. Actuators B Chem.* **2020**, *320*, 128367, doi:10.1016/j.snb.2020.128367. [[CrossRef](#)]
8. Raether, H. *Surface Plasmons on Smooth and Rough Surfaces and on Gratings*; Springer: Berlin/Heidelberg, Germany, 1988.
9. Baryshev, A.; Merzlikin, A.; Inoue, M. Efficiency of optical sensing by a plasmonic photonic-crystal slab. *J. Phys. D Appl. Phys.* **2013**, *46*, 125107. [[CrossRef](#)]
10. Ignatov, A.I.; Merzlikin, A.M. Two optical sensing elements for H₂O and NO₂ gas sensing based on the single plasmonic–photonic crystal slab. *Adv. Opt. Technol.* **2020**, *9*, 203–208. [[CrossRef](#)]
11. Berini, P.; De Leon, I. Surface plasmon–polariton amplifiers and lasers. *Nat. Photonics* **2012**, *6*, 16–24. [[CrossRef](#)]

12. Gorham, W.F. A new, general synthetic method for the preparation of linear poly-p-xylylenes. *J. Polym. Sci. Part A-1 Polym. Chem.* **1966**, *4*, 3027–3039. [[CrossRef](#)]
13. Valentini, L.; Biagiotti, J.; Kenny, J.; Santucci, S. Effects of single-walled carbon nanotubes on the crystallization behavior of polypropylene. *J. Appl. Polym. Sci.* **2003**, *87*, 708–713. [[CrossRef](#)]
14. Chae, D.W.; Hong, S.M. Dynamic crystallization behavior, morphology, and physical properties of highly concentrated poly (vinylidene fluoride)/silver nanocomposites. *J. Polym. Sci. Part B Polym. Phys.* **2010**, *48*, 2379–2385. [[CrossRef](#)]
15. Mamunya, Y.P.; Davydenko, V.; Pissis, P.; Lebedev, E. Electrical and thermal conductivity of polymers filled with metal powders. *Eur. Polym. J.* **2002**, *38*, 1887–1897. [[CrossRef](#)]
16. Hetland, Ø.S.; Maradudin, A.A.; Nordam, T.; Simonsen, I. Numerical studies of the scattering of light from a two-dimensional randomly rough interface between two dielectric media. *Phys. Rev. A* **2016**, *93*, 053819. [[CrossRef](#)]
17. Turbil, C.; Yoo, T.S.H.; Simonsen, I.; Teisseire, J.; Gozhyk, I.; Garcia-Caurel, E. Experimental studies of the transmission of light through low-coverage regular or random arrays of silica micropillars supported by a glass substrate. *Appl. Opt.* **2019**, *58*, 9267–9278. [[CrossRef](#)]
18. Sánchez-Gil, J.; Maradudin, A.; Lu, J.Q.; Freilikher, V.; Pustilnik, M.; Yurkevich, I. Scattering of electromagnetic waves from a bounded medium with a random surface. *Phys. Rev. B* **1994**, *50*, 15353. [[CrossRef](#)] [[PubMed](#)]
19. Wang, Z.L.; Ogura, H.; Takahashi, N. Enhanced scattering from a planar waveguide structure with a slightly rough boundary. *Phys. Rev. B* **1995**, *52*, 6027. [[CrossRef](#)]
20. Garcia, R. Radiative transfer with polarization in a multi-layer medium subject to Fresnel boundary and interface conditions. *J. Quant. Spectrosc. Radiat. Transf.* **2013**, *115*, 28–45. [[CrossRef](#)]
21. Aduiev, B.; Nurmukhametov, D.; Belokurov, G.; Zvekov, A.; Kalenskii, A.; Nikitin, A.; Liskov, I.Y. Integrating sphere study of the optical properties of aluminum nanoparticles in tetranitropentaerythrite. *Tech. Phys.* **2014**, *59*, 1387–1392. [[CrossRef](#)]
22. Puzko, R.; Kozlov, D.; Fabelinsky, V.; Polivanov, Y.; Smirnov, V.; Sarychev, A.; Ryzhikov, I.; Bandarenka, H.; Merzlikin, A. Incoherent scattering from dielectric metasurfaces under the influence of electromagnetic eigenmodes. *Opt. Express* **2019**, *27*, 21701–21716. [[CrossRef](#)]
23. Gorodnichev, E.; Dudarev, S.; Rogozkin, D.; Ryazanov, M. Nature of anomalous x-ray reflection from a surface. *Jetp Lett.* **1988**, *48*, 147–150.
24. Ramirez-Duverger, A.S.; Garcia-Llamas, R. Light scattering from a multimode waveguide of planar metallic walls. *Opt. Commun.* **2003**, *227*, 227–235. [[CrossRef](#)]
25. Ramakrishnan, G.; Planken, P.C. Percolation-enhanced generation of terahertz pulses by optical rectification on ultrathin gold films. *Opt. Lett.* **2011**, *36*, 2572–2574. [[CrossRef](#)] [[PubMed](#)]
26. Brouers, F.; Blacher, S.; Sarychev, A.K. Giant field fluctuations and anomalous light scattering from semicontinuous metal films. *Phys. Rev. B* **1998**, *58*, 15897. [[CrossRef](#)]
27. Breit, M.; Podolskiy, V.; Grésillon, S.; Von Plessen, G.; Feldmann, J.; Rivoal, J.; Gadenne, P.; Sarychev, A.K.; Shalaev, V.M. Experimental observation of percolation-enhanced nonlinear light scattering from semicontinuous metal films. *Phys. Rev. B* **2001**, *64*, 125106. [[CrossRef](#)]
28. Bepalov, V.; Boginskaya, I.; Bykov, I.; Vinogradov, A.; Gusev, A.; Dorofeenko, A.; Mailyan, K.; Ryzhikov, I.; Pebalk, A. Using the metal-polymer nanocomposite polyparaxylylene-Ag as a medium with assigned optical characteristics. *J. Opt. Technol.* **2010**, *77*, 726–728. [[CrossRef](#)]
29. Streltsov, D.R.; Mailyan, K.A.; Gusev, A.V.; Ryzhikov, I.A.; Erina, N.A.; Su, C.; Pebalk, A.V.; Ozerin, S.A.; Chvalun, S.N. Electrical properties, structure, and surface morphology of poly (p-xylylene)-silver nanocomposites synthesized by low-temperature vapor deposition polymerization. *Appl. Phys. A* **2013**, *110*, 413–422. [[CrossRef](#)]
30. Afanasev, K.N.; Boginskaya, I.A.; Dorofeenko, A.V.; Gysev, A.V.; Mailyan, K.A.; Pebalk, A.V.; Chvalyn, V.N.; Ozerin, S.A.; Sedova, M.V.; Rodionov, I.A.; et al. Poly (p-xylylene) silver nanocomposites: Optical, radiative, and structural properties. *IEEE Trans. Nanotechnol.* **2017**, *16*, 274–280. [[CrossRef](#)]
31. Gazicki, M.; Surendran, G.; James, W.; Yasuda, H. Polymerization of para-xylylene derivatives (parylene polymerization). III. Heat effects during deposition of parylene N at different temperatures. *J. Polym. Sci. Part A Polym. Chem.* **1986**, *24*, 215–240. [[CrossRef](#)]

32. Streltsov, D.R.; Buzin, A.I.; Dmitryakov, P.V.; Kamasa, P.; Ivanov, D.A.; Chvalun, S.N. A study of p-xylylene polymerization kinetics using high-vacuum in situ differential scanning calorimetry. *Thermochim. Acta* **2016**, *643*, 65–72. [[CrossRef](#)]
33. Yeh, P. Matrix formulation for isotropic layered media. In *Optical Waves in Layered Media*; John Wiley & Sons: New Jersey, NJ, USA, 2005; pp. 102–118.
34. Hlídek, P.; Biederman, H.; Choukourov, A.; Slavínská, D. Behavior of Polymeric Matrices Containing Silver Inclusions, 1–Review of Adsorption and Oxidation of Hydrocarbons on Silver Surfaces/Interfaces as Witnessed by FT-IR Spectroscopy. *Plasma Process. Polym.* **2008**, *5*, 807–824. [[CrossRef](#)]
35. Sarychev, A.K.; Shubin, V.; Shalaev, V.M. Anderson localization of surface plasmons and nonlinear optics of metal-dielectric composites. *Phys. Rev. B* **1999**, *60*, 16389. [[CrossRef](#)]
36. Novotny, L.; Hecht, B. *Principles of Nano-Optics*; Cambridge University Press: Cambridge, UK, 2012.

Publisher’s Note: MDPI stays neutral with regard to jurisdictional claims in published maps and institutional affiliations.



© 2020 by the authors. Licensee MDPI, Basel, Switzerland. This article is an open access article distributed under the terms and conditions of the Creative Commons Attribution (CC BY) license (<http://creativecommons.org/licenses/by/4.0/>).